Contrib Mineral Petrol (2008) 155:45–61
DOI 10.1007/s00410-007-0223-7

ORIGINAL PAPER

Shallow-level decompression crystallisation and deep magma supply at Shiveluch Volcano

M. C. S. Humphreys · J. D. Blundy · R. S. J. Sparks

Received: 9 January 2007 / Accepted: 18 May 2007 / Published online: 14 June 2007

Abstract Recent petrological studies indicate that some crustal magma chambers may be built up slowly by the intermittent ascent and amalgamation of small packets of magma generated in a deep-seated source region. Despite having little effect on whole-rock compositions, this process should be detectable as variable melt trace element composition, preserved as melt inclusions trapped in phenocrysts. We studied trace element and H_2O contents of plagioclase- and hornblende-hosted melt inclusions from andesite lavas and pumices of Shiveluch Volcano, Kamchatka. Melt inclusions are significantly more evolved than the whole rocks, indicating that the whole rocks contain a significant proportion of recycled foreign material. H_2O concentrations indicate trapping at a wide range of pressures, consistent with shallow decompression-driven crystallisation. The variation of trace element concentrations indicates up to ~30% decompression crystallisation, which accounts for crystallisation of the groundmass and rims on phenocrysts. Trace element scatter could be explained by episodic stalling during shallow magma ascent, allowing incompatible element concentrations to increase during isobaric crystallisation. Enrichment of Li at intermediate pH_2O reflects influx and condensation of metal-rich vapours. A set of ''exotic melts'', identified by their anomalous incompatible trace element characteristics, indicate variable source chemistry. This is consistent with evolution of individual magma batches with small differences in trace element chemistry, and intermittent ascent of magma pulses.

Keywords Melt inclusions · Decompression crystallisation · Shiveluch · Exotic melts · Degassing

Communicated by J. Hoefs.

Electronic supplementary material The online version of this article (doi:10.1007/s00410-007-0223-7) contains supplementary material, which is available to authorized users.

M. C. S. Humphreys (✉)
Department of Earth Sciences, University of Cambridge,
Downing Street, Cambridge CB2 3EQ, UK
e-mail: mcsh2@cam.ac.uk

M. C. S. Humphreys · J. D. Blundy · R. S. J. Sparks
Department of Earth Sciences, University of Bristol,
Wills Memorial Building, Queen's Road,
Bristol BS8 1RJ, UK

Introduction

Melt inclusions trapped in phenocrysts can provide an insight into the processes acting during evolution of residual melt and volatiles during magma crystallisation. For example, incompatible trace element concentrations are related to the degree of fractionation, and to magma source characteristics. Volatile elements and light trace metals can provide information about shallow-level degassing processes. Combined with whole-rock data, melt inclusions can thus give information about different stages of magma evolution, from deep source to eruption.

Crystallisation of volatile-saturated magma can be induced by two end-member mechanisms: external cooling at constant pressure (isobaric cooling), or exsolution of volatiles during ascent (polybaric degassing), though intermediate scenarios such as episodic, stop-start ascent are also possible. The solubility of H_2O and other volatiles depends on pressure (e.g. Zhang 1999), so H_2O-saturated ascent results in exsolution and degassing. This promotes a large increase in liquidus temperature, resulting in significant magma undercooling and copious crystallisation (e.g.

Sparks and Pinkerton 1978; Swanson et al. 1989; Cashman 1992; Geschwind and Rutherford 1995; Sparks et al. 2000; Blundy and Cashman 2001, 2005). Decompression-induced crystallisation is rapid (e.g. Sparks and Pinkerton 1978; Berlo et al. 2004) and results in decreasing melt H_2O, increasing melt SiO_2, and increasing crystal and bubble contents of the magma. These factors cause rheological stiffening in degassing magma, and viscosity increases of several orders of magnitude (e.g. Sparks 1997). The increase in viscosity can result in magma pressurisation in the upper parts of the conduit, and may play a role in the unpredictable transitions between stable dome growth and potentially powerful explosions (Barmin et al. 2002; Melnik and Sparks 2005). Determining the different crystallisation mechanisms for a magmatic system can thus provide information about eruption dynamics, corresponding precursory activity and hazards.

Melt inclusions may also preserve subtle variations in melt chemistry, reflecting source characteristics in a way that is masked in whole-rock compositions. Magma batches of different compositions may enter the sub-volcanic system, but if their volumes are small relative to the host magma, significant variations in whole-rock geochemistry may not be observed (Eichelberger et al. 2006; Humphreys et al. 2006a). However, distinct trace element signatures of different magma batches could be preserved in the residual melt, and therefore detected in melt inclusions.

In this study we present melt inclusion data from plagioclase and hornblende phenocrysts from the 2001 to 2004 eruption of Shiveluch Volcano, Kamchatka. We use these data to evaluate the role of crystallisation driven by decompression and H_2O-loss, with reference to petrological observations. A subset of ''exotic melts'' is identified on the basis of their trace element compositions, and are used to infer processes relating to ascent and mixing of chemically distinct magma batches from depth.

Geological background

Shiveluch Volcano forms an isolated massif in the northern part of the Central Kamchatka Depression, close to the intersection of the Kurile and Kamchatka arcs. Shiveluch is a large stratovolcano with over 60 explosive eruptions during the Holocene (Dirksen et al. 2006). The current eruption of Shiveluch began in 2001 and is typified by periods of strong dome growth, accompanied by explosions of varying intensity, and separated by periods of slow, stable dome growth accompanied by steaming (Dirksen et al. 2006). In this study, we focus on dome rocks and pumices generated by explosions during the early part of the recent eruption.

The samples studied are porphyritic, medium-K andesites (61–63 wt% SiO_2). Their petrology is complex, with diverse phenocryst zoning, as described in Humphreys et al. (2006a). The rocks contain 26–52 vol% phenocrysts, dominated by euhedral plagioclase and hornblende, with minor Fe-Ti oxides and orthopyroxene (Dirksen et al. 2006). Hornblende phenocrysts are pristine and do not show rims of breakdown products, though occasional rounded crystal boundaries provide some evidence for resorption. Apatite and anhydrite are present as microphenocrysts and as inclusions in phenocrysts. Xenocrysts of olivine, orthopyroxene and clinopyroxene are present and commonly display well-developed reaction rims (Dirksen et al. 2006; Humphreys et al. 2006a). Melt inclusions are common in both hornblende and plagioclase. The groundmass typically contains microlites of plagioclase, pyroxenes and titanomagnetites, which together account for up to ~30% by volume of the groundmass of dome rocks. Matrix glasses are silica-rich (typically 77.5–79.5 wt% SiO_2 on an anhydrous basis) and H_2O-poor.

Analytical methods

Sample preparation

Studies of melt inclusions typically involve rigorous and very time-consuming sample preparation. Each inclusion to be analysed is observed individually and texturally characterised, then exposed by polishing. The aim of this approach is to identify and study only those inclusions deemed on petrographic grounds to be primary. While this approach is very useful for minerals such as quartz and olivine, melt inclusions in minerals such as hornblende and plagioclase show such a diversity of texture and 3D morphology that a simple textural classification is rarely unequivocal and could lead to valuable information being lost.

We used a more direct method (after Blundy and Cashman 2005). Several hundred grains were mounted together and polished, and any exposed inclusions were analysed. Inclusions were observed petrographically after polishing, and textural features (shape, size, presence of bubbles, daughter minerals etc.) were noted (Supplementary Table 1), with the *caveat* that some information might have been lost during polishing. This method of sample preparation allows hundreds of inclusions to be analysed relatively quickly, giving a comprehensive overview of a whole population of melt inclusions. This would not be available from a few analyses using standard preparation methods. Prior petrographic observation can also be difficult when the host mineral is very dark (e.g. hornblende). Our principal objective was to obtain information from inclusions of all textural types, without *a priori* discrimination on textural grounds.

Phenocrysts of hornblende and plagioclase were hand-picked from lightly crushed samples, mounted in Buehler EpoThin® cold-cure resin and singly polished to expose melt inclusions. Major element concentrations of all inclusions were measured using electron probe micro-analysis (EPMA). A subset of inclusions was then analysed for H_2O and trace elements by secondary ion mass spectrometry (SIMS).

Electron probe micro-analysis

Major and minor element concentrations of 214 glasses were analysed using a CAMECA SX-100 five spectrometer instrument at the University of Bristol. A 15 μm, defocused spot was used with a 2 nA, 15 kV beam to minimise Na loss during analysis (Humphreys et al. 2006b). Routine primary standards were used for calibration, together with well-characterised secondary glass standards as described in Humphreys et al. (2006b). Typical analytical errors are given in Supplementary Table 1. H_2O contents of glasses estimated as ''volatiles by difference'' have a typical precision of ~0.8 wt% (2σ), and average absolute deviation from SIMS H_2O values of approximately 0.6 wt% (see also Devine et al. 1995; Humphreys et al. 2006b). P and Cl were analysed in a subset of inclusions, using a 10 nA, 15 kV beam. F and S are below detection limits (~200 ppm S; ~0.22 wt% F) under these conditions.

Secondary ion mass spectrometry

A subset of 84 melt inclusions (20 in hornblende and 64 in plagioclase) and 7 matrix glasses was analysed for isotopes of light trace elements ($^{7}Li^{+}$, $^{9}Be^{+}$, $^{11}B^{+}$, $^{45}Sc^{+}$, $^{47}Ti^{+}$ and $^{51}V^{+}$) and $^{1}H^{+}$ using a CAMECA ims-4f instrument at the University of Edinburgh, using procedures described in Blundy and Cashman (2005). The instrument was controlled by Charles Evans and Associates PXT interface and software. A further subset of 31 inclusions (24 in plagioclase and 7 in hornblende) and 5 matrix glasses was analysed for isotopes of heavy trace elements ($^{85}Rb^{+}$, $^{88}Sr^{+}$, $^{89}Y^{+}$, $^{90}Zr^{+}$, $^{93}Nb^{+}$, $^{133}Cs^{+}$, $^{138}Ba^{+}$, $^{139}La^{+}$, $^{140}Ce^{+}$, $^{141}Pr^{+}$, $^{143}Nd^{+}$, $^{149}Sm^{+}$, $^{232}Th^{+}$ and $^{238}U^{+}$).

The diameter of the ion beam was typically ~12–15 μm for light elements and ~20–25 μm for heavy trace elements. The beam was manually aimed onto the melt inclusion, which was usually visible using an inclined, reflected light microscope with a 1.7 mm field of view. In large melt inclusions, the heavy and light trace element analyses were conducted at separate points in the inclusion. In smaller inclusions with insufficient space to allow two separate spots, both analyses were conducted on exactly the same area of the inclusion. Typical uncertainties are <0.15 wt% for H_2O and ≤ 10% relative for trace elements.

Textural characteristics of melt inclusions

Melt inclusions can be trapped during primary crystallisation of the host phenocryst, or during reaction, resorption or partial dissolution of the host (e.g. Lowenstern 2003). After trapping, the chemistry and shape of the inclusion may alter as a result of post-entrapment modification processes and re-equilibration with the host phenocryst. Each melt inclusion must therefore be studied in the context of the textures observed in its host crystal.

Inclusions that are trapped during simple crystal growth vary from rounded to a euhedral ''negative-crystal'' shape (Fig. 1a). This probably reflects the degree of re-equilibration with the host phenocryst: inclusions tend towards euhedral, negative-crystal shapes after long periods at high temperatures (Clocchiatti 1975). This textual re-equilibration process does not alter the composition of the melt inclusion (Frezzotti 2001), unless also accompanied by crystallisation. In contrast, partial dissolution of plagioclase or hornblende phenocrysts (e.g. during H_2O-undersaturated decompression; Holtz and Johannes 1994; Humphreys et al. 2006a) results in highly irregular, corroded crystal cores that can easily trap melt when crystallisation resumes. Inclusions trapped in this way fill the irregular or elongate voids formed during dissolution, and often cross-cut several zones in the crystal (Fig. 1e).

In transmitted light, inclusions are pale mauve to pale brown, and most contain a vapour bubble (Fig. 1a). The volume proportion of negative-crystal inclusions occupied by the bubble is roughly constant at a few (~3–8) percent. Bubble volumes in hornblende-hosted inclusions are smaller. The bubble volume proportion in irregular inclusions appears to vary. This may simply be due to the complicated inclusion geometry, or could reflect different cooling histories or heterogeneous trapping (Lowenstern 2003). In plagioclase, melt inclusions sometimes occur in zones corresponding to the shape of compositional zoning, though these inclusions are typically too small to analyse (e.g. oscillatory plagioclase, Fig. 1b). More commonly, inclusions exhibit no obvious zonal arrangement. In hornblende, inclusion-rich zones are also seen (Fig. 1c), but most inclusions have no obvious spatial arrangement (Fig. 1d).

Sieve-textured plagioclase phenocrysts contain a network of μm-scale melt channels resulting from reaction with hotter, mafic melt (Tsuchiyama 1985; Nakamura and Shimakita 1998). These are crystallographically controlled, commonly rimmed with calcic plagioclase, and may be partially occluded by orthopyroxene. These reaction-derived melt channels were not analysed in this study.

Glassy melt inclusions were identified in plagioclase and hornblende phenocrysts from crystal-rich silicic andesite lavas and pumices from the 2001 to 2004 eruption of

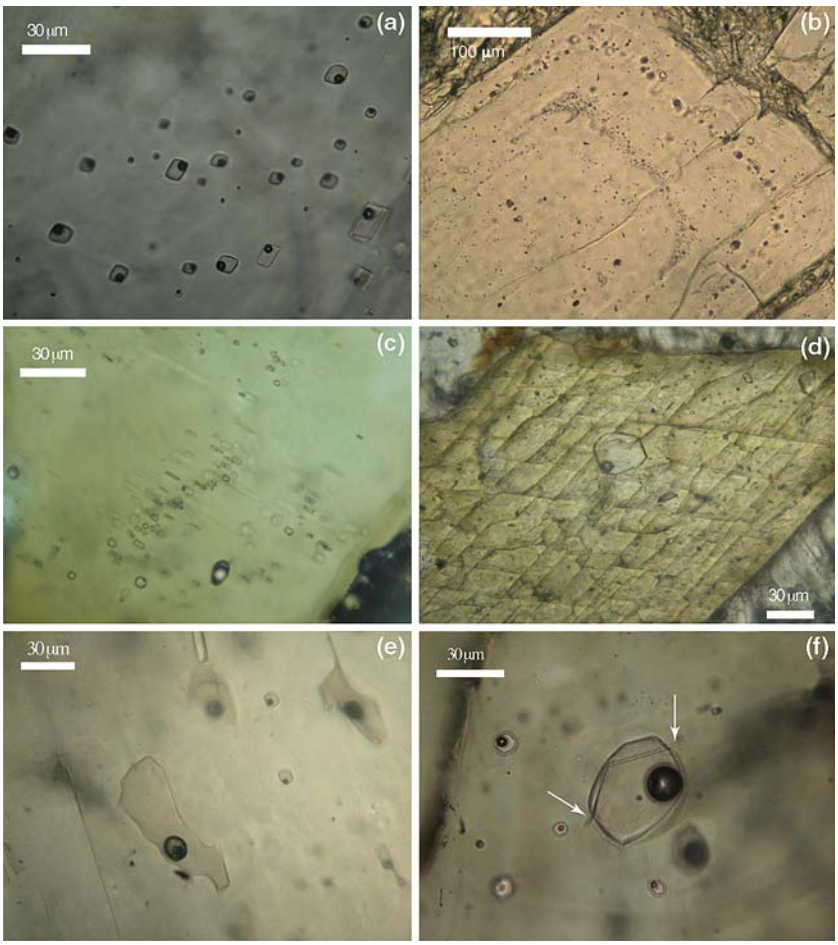

Fig. 1 Photomicrographs of typical melt inclusions in plagioclase and hornblende phenocrysts in Shiveluch magmas. **a** Zone of typical ''negative crystal'' shaped inclusions in plagioclase, with approximately constant bubble volume proportions. **b** Zonal distribution of melt inclusions corresponds with oscillatory zonation in the phenocryst. **c** Clear zonal arrangement of tiny negative-crystal melt inclusions in hornblende. **d** Isolated, euhedral melt inclusion in hornblende. **e** Irregular inclusion in core of plagioclase phenocryst. **f** Large inclusion in plagioclase contains two apatite needles (*white arrows*) which intrude the inclusion from the host crystal

Shiveluch Volcano (Supplementary Table 1; Humphreys et al. 2006a). In total 203 inclusions were analysed (111 in hornblende and 92 in plagioclase), together with 11 matrix glasses. The majority of inclusions analysed did not contain any daughter mineral. Approximately 45% contained a bubble. The size of the inclusions analysed varied from ~18 to ~145 μm along the maximum dimension. The volatile contents and major element compositions of inclusions are not related to their textural characteristics, i.e. size or presence of a fluid bubble (Supplementary Table 1).

Post-entrapment modification of inclusions

Melt inclusion compositions may be unrepresentative of the original melt composition if there has been significant post-entrapment modification of the inclusion. The most common forms of modification are mineralisation, continued crystallisation at the inclusion interface, and volatile leakage. Diffusive re-equilibration of the inclusion with the host melt, occurring through the crystal itself (Qin et al. 1992; Gaetani and Watson 2000) is considered unimportant in view of the rapid magma ascent rate and expected low diffusivities in plagioclase and hornblende. Post-entrapment modification may be an open-system process, where chemical components are exchanged between inclusion and matrix along melt channels, possibly with concomitant precipitation of the host mineral, or a closed-system process. Examples of closed-system post-entrapment processes are growth of the host mineral on the walls of the inclusion, or precipitation of new daughter minerals.

Some inclusions observed in hornblende contain small ''daughter'' crystals of plagioclase, orthopyroxene, clinopyroxene, titanomagnetite or apatite. The extent of mineralisation can vary from a small microlite forming a minor proportion of the inclusion, to almost complete occlusion by plagioclase or orthopyroxene. In contrast, daughter mineralisation in plagioclase-hosted inclusions is rare. Where daughter mineralisation is present, a single apatite needle commonly intrudes from the host plagioclase into the inclusion (Fig. 1f). It is not clear whether these crystals were trapped together with the melt or grew subsequent to entrapment of the melt inclusion (e.g. Roedder 1984), though we note that needles of apatite are abundant as inclusions in plagioclase. Analysis of partially mineralised inclusions was avoided wherever possible.

Closed-system growth of the host at the margins of the inclusions may be suspected if inclusion populations from different host minerals follow separate compositional trends (Cottrell et al. 2002). If this is the case, the original melt composition can be reconstructed graphically (Watson 1976). However, all inclusions analysed in hornblende and plagioclase are high-SiO_2 rhyolite, and follow very similar compositional trends. This independence of host mineral composition implies a lack of significant closed-system post-entrapment crystallisation of the host (as distinct from mineralisation). When plagioclase-hosted inclusions are reconstructed prior to $\leq 5\%$ post-entrapment crystallisation of plagioclase, the chemistry of both inclusion populations coincides (see Fig. 2). We are therefore satisfied that only a small amount (<5%) of post-entrapment crystallisation has occurred. This is also consistent with the conclusions of Tolstykh et al. (2000). Plagioclase-hosted inclusions presented in figures are reconstructed prior to 5% plagioclase (An_{45}) post-entrapment crystallisation.

Melt inclusion chemistry

Major element compositions

Figure 2 shows major-element compositional variation in whole-rocks (Dirksen et al. 2006; Humphreys et al. 2006a) and melt inclusions from the 2001 to 2004 eruption, together with whole-rock data from previous eruptions for comparison (Tolstykh et al. 2000; Martin 2001; Melekestsev et al. 1991; Pineau et al. 1999; Hochstaedter et al. 1996; Ishikawa et al. 2001; Kepezhinskas et al. 1997; Volynets et al. 1997). The currently erupted lavas are silicic hornblende-plagioclase andesites with 61–63 wt% SiO_2, and plot at the end of the trend defined by older eruptions. Thus there is a compositional gap of 8 wt% SiO_2 between the most primitive melt inclusions (rhyodacite) and the most evolved whole-rocks (silicic andesite) (see also Naumov et al. 1997; Humphreys et al. 2006a). A similar feature can be observed in other arc magmas (e.g. Vulcano, Italy: Gioncada et al. 1998; Dominica, W. Indies: Gurenko et al. 2005; Mount St Helens, USA: Blundy and Cashman 2005). The extrapolated linear co-variations of oxides from melt inclusions and whole rocks have different slopes, and intersect within the compositional gap at ~67–70 wt% SiO_2 (Fig. 2).

The melt inclusions form a continuous series in major element composition (Supplementary Table 1), ranging from 72.0 to 78.7 wt% SiO_2(n), where (n) denotes normalised to 100% anhydrous. Matrix glasses constitute some of the most evolved compositions (76.7–79.4 wt% SiO_2). SiO_2 correlates negatively with Al_2O_3, CaO, Na_2O and MgO, and positively with TiO_2 and K_2O (Fig. 2). FeO decreases slightly with increasing SiO_2; MgO contents are relatively constant but scattered (Fig. 2). MgO correlates with FeO, with matrix glasses showing the lowest concentrations. A few plagioclase-hosted inclusions extend to high CaO (Fig. 2); this may be a result of minor (5%) analysis overlap with the host plagioclase. Most of the major-element trends are consistent with crystallisation of groundmass, dominated by plagioclase. However, decreasing Na_2O implies extraction of a phase very rich in Na, and cannot be explained solely by plagioclase-dominated crystallisation (see below).

There is a subtle compositional difference between melt inclusions trapped in hornblende and those in plagioclase phenocrysts. Hornblende-hosted inclusions have systematically lower MgO and higher FeO concentrations than plagioclase-hosted inclusions (Fig. 3), even after correction for the small amount (5%) of post-entrapment crystallisation of plagioclase. The anomalously high FeO and low MgO in hornblende-hosted inclusions are not consistent with the effects of post-entrapment crystallisation of hornblende.

H_2O concentrations

H_2O concentrations, measured by SIMS, range from 0 to 5.1 wt% in the melt inclusions (Supplementary Table 1). Matrix glasses contain 0.1 to 0.2 wt% H_2O. Inclusions in plagioclase clearly show decreasing H_2O with increasing SiO_2 (Fig. 4). Matrix glasses plot at the high-SiO_2, low-H_2O end of this trend. Hornblende-hosted melt inclusions cover the same range of H_2O contents as plagioclase-hosted inclusions, but some plot below the H_2O–SiO_2 curve defined by the plagioclase-hosted inclusions. This could result from loss of H_2O, either during the eruption or by leakage from the inclusions. H_2O also correlates with other major elements (Fig. 4). Na_2O and FeO show a change in behaviour at low H_2O, with concentrations dropping rapidly to the level in the matrix glasses.

Li, Cl, Be and B

Li concentrations in melt inclusions vary widely, from 11 to 118 ppm (Supplementary Table 2); matrix glasses contain 9 to 17 ppm. Li contents of hornblende-hosted inclusions decrease with increasing SiO_2, and increase with H_2O, but inclusions in plagioclase show wide scatter, and enrichment of Li at intermediate H_2O contents (Fig. 5a).

Cl concentrations range from ~900 to 2,400 ppm (Supplementary Table 1), and show a slight increase with decreasing H_2O (Fig. 5b). This is consistent with higher solubility in the melt at low pressure (Metrich and Rutherford 1992) and the incompatible nature of Cl during crystallisation. A few inclusions show high Cl, though there is no correlation with the enrichment of Li.

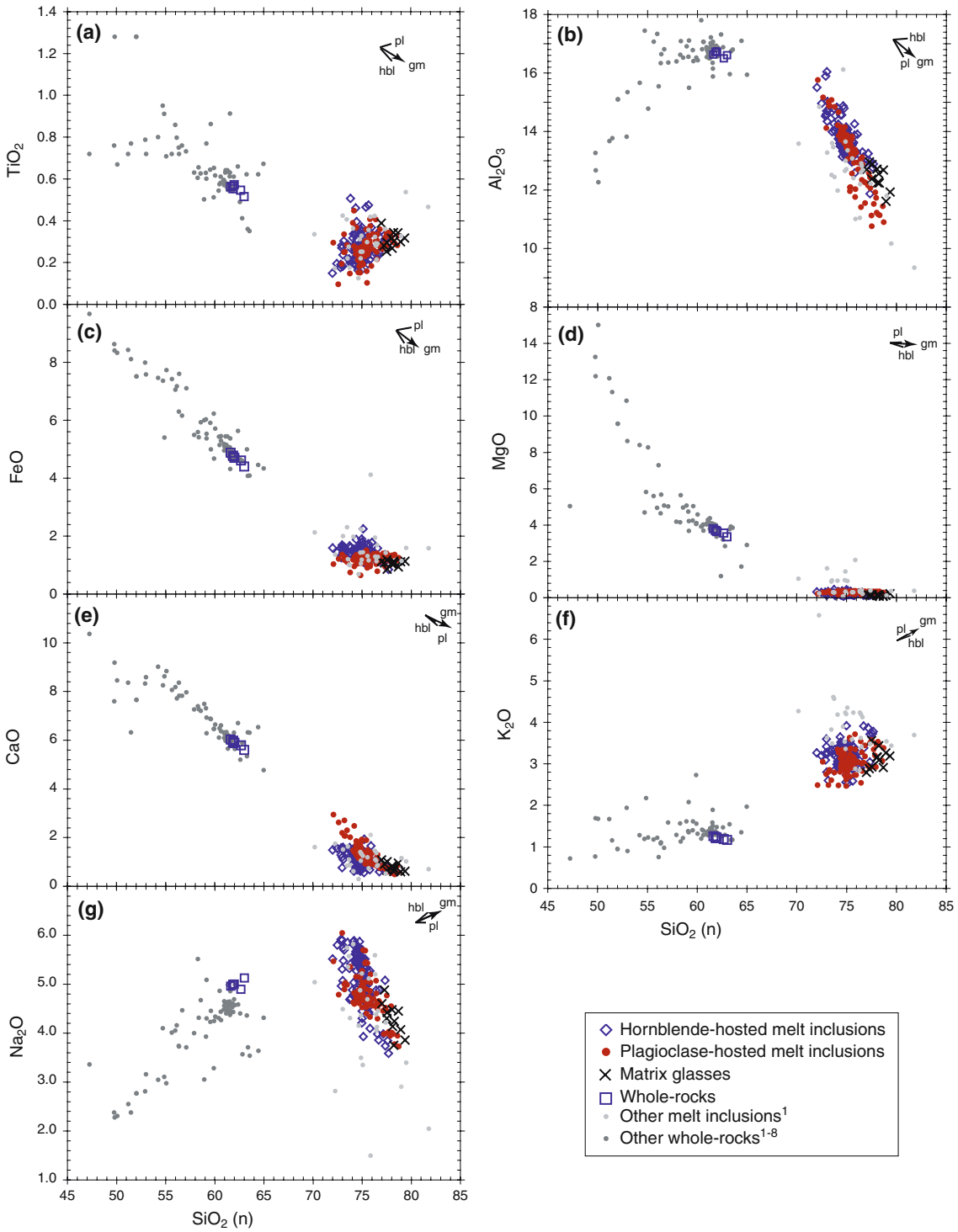

Fig. 2 Major element compositions (wt% anhydrous) of melt inclusions analysed by EPMA. *Large filled circles* indicate melt inclusions in plagioclase, *hollow diamonds* indicate melt inclusions in hornblende, *crosses* indicate matrix glasses. Plagioclase-hosted inclusions have been reconstructed prior to 5% post-entrapment crystallisation of An_{45}. *Lines* give approximate vectors for 5% crystallisation of plagioclase (*pl*) and hornblende (*hbl*); *arrow* indicates 10% groundmass crystallisation. Whole-rock data (*squares*) for the 2001–2004 eruption are also shown (Dirksen et al. 2006). *Light grey and dark grey filled circles* represent Shiveluch melt inclusions and whole rock data from previous studies: [1]Tolstykh et al. (2000); [2]Martin 2001; [3]Melekestsev et al. 1991; [4]Pineau et al. 1999; [5]Hochstaedter et al. 1996; [6]Ishikawa et al. 2001; [7]Kepezhinskas et al. 1997; [8]Volynets et al. 1997

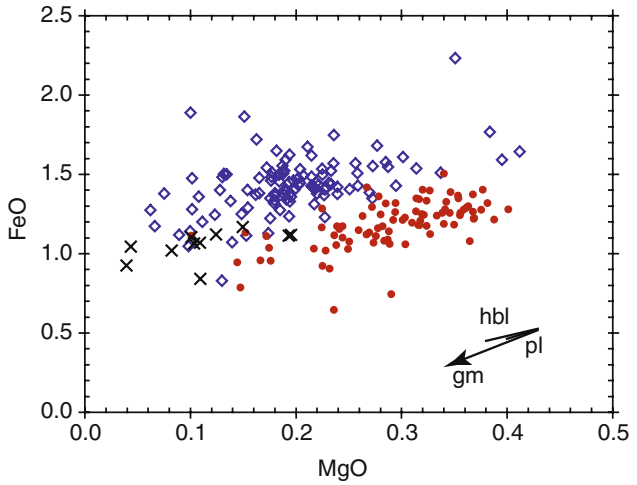

Fig. 3 FeO and MgO concentrations (wt%) in melt inclusions. Hornblende-hosted inclusions have higher FeO and lower MgO than those in reconstructed plagioclase-hosted inclusions. *Lines* give approximate vectors for crystallisation of hornblende (1%) and plagioclase (5%); *arrow* indicates 5% groundmass crystallisation (*gm*). *Symbols* as Fig. 2

Be concentrations are low (Supplementary Table 2), and show similar behaviour to Cl, with increasing Be as H_2O decreases (Fig. 5c). Several inclusions show anomalously high Be at intermediate H_2O contents (Fig. 5c). Be concentrations in the matrix glass are slightly lower than the most evolved melt inclusions (Fig. 5c).

B contents of most melt inclusions range from ~50 to ~80 ppm (Supplementary Table 2), and are not correlated with H_2O or SiO_2 (Fig. 5d). Matrix glasses contain 50–70 ppm. Several inclusions in plagioclase have anomalously high B (up to 175 ppm).

Trace element chemistry

Melt inclusions form scattered trends of trace elements, and cover a much greater range of concentrations than whole-rocks from the same eruption (Fig. 6; Supplementary Table 2). These variations are beyond analytical error. Sr concentrations decrease with increasing SiO_2, consistent with crystallisation dominated by plagioclase. V also decreases strongly with SiO_2; this probably results from crystallisation of hornblende, or Fe-Ti oxides in the groundmass. Immobile, incompatible trace elements (Zr, Nb) increase with increasing SiO_2 (Fig. 6). Large ion lithophile (LIL) elements (e.g. Rb, Ba) have no clear relationship with SiO_2 or H_2O but tend to correlate well with other elements with similar partitioning characteristics (Fig. 7). Trace element concentrations in the whole-rocks define trends with different slope to the melt inclusions (Figs. 6, 7). On a trace element variation diagram (Fig. 8), the main inclusion population shows a typical arc signature of high LILE (Gill 1981), and negative anomalies for Nb and Ti.

Several melt inclusions have trace element characteristics that fall outside the broad band defined by the main populations of inclusions. These inclusions are identified as ''exotic melts'' since they show trace element concentrations up to five times higher than the main inclusion population. Their host crystals are of various textural types, may show patchy or oscillatory zoning, and are indistinguishable texturally from other phenocrysts hosting ''normal'' inclusions. The inclusions themselves have no unusual textural characteristics (see Supplementary Table 1).

The exotic melt inclusions comprise two sets. The first set (m12s22-3, m12s26-3, m12s25-3) has very low U (<0.01 ppm) and U/Th, but otherwise normal trace element characteristics (Fig. 8).

The second group of inclusions has concentrations of high field strength (HFS) elements (Nb, Zr, Th, U) that vary from depleted (m14s47-1) to strongly enriched (e.g. m1s33-1, m16s20033-1) compared with the main population (Fig. 8). These inclusions typically plot away from the trend defined by the main population of inclusions and are thus easily recognised on element and ratio plots (Figs. 7, 9). In particular, inclusions m1s33-1 and m16s20033-1 have high Nb/La and low Ba/Th, while m14s47-1 shows the opposite characteristics. B concentrations correlate with Nb/La (Fig. 9). Inclusion m15shv1-3 is enriched in rare earth elements (REE), but has normal Zr, Ti and Th.

Discussion

The melt inclusions are considerably more silica-rich than their whole-rocks, with SiO_2(n) up to 80 wt%. These very high SiO_2 concentrations can only be produced if the melt equilibrates at very low pressures (Tuttle and Bowen 1958; Cashman and Blundy 2000). This implies that the latest stages of crystallisation, which the melt inclusions record, occurred at shallow pressure. The ''compositional gap'' between whole-rocks and melt inclusions is hard to reconcile with continuous fractional crystallisation. Instead, we infer that the phenocrysts in which the inclusions are trapped crystallise from a dacitic melt, while the more SiO_2-poor whole-rock compositions reflect mixing of this melt with other magmas, remobilised cumulate materials and crystals incorporated from previous eruptive or intrusive episodes (Naumov et al. 1997; Dungan et al. 2001; Eichelberger et al. 2005; Humphreys et al. 2006a). The marked inflection between whole-rock and melt inclusion trends (see Fig. 3) reflects a change from the higher-pressure crystallisation processes which produce the dacitic

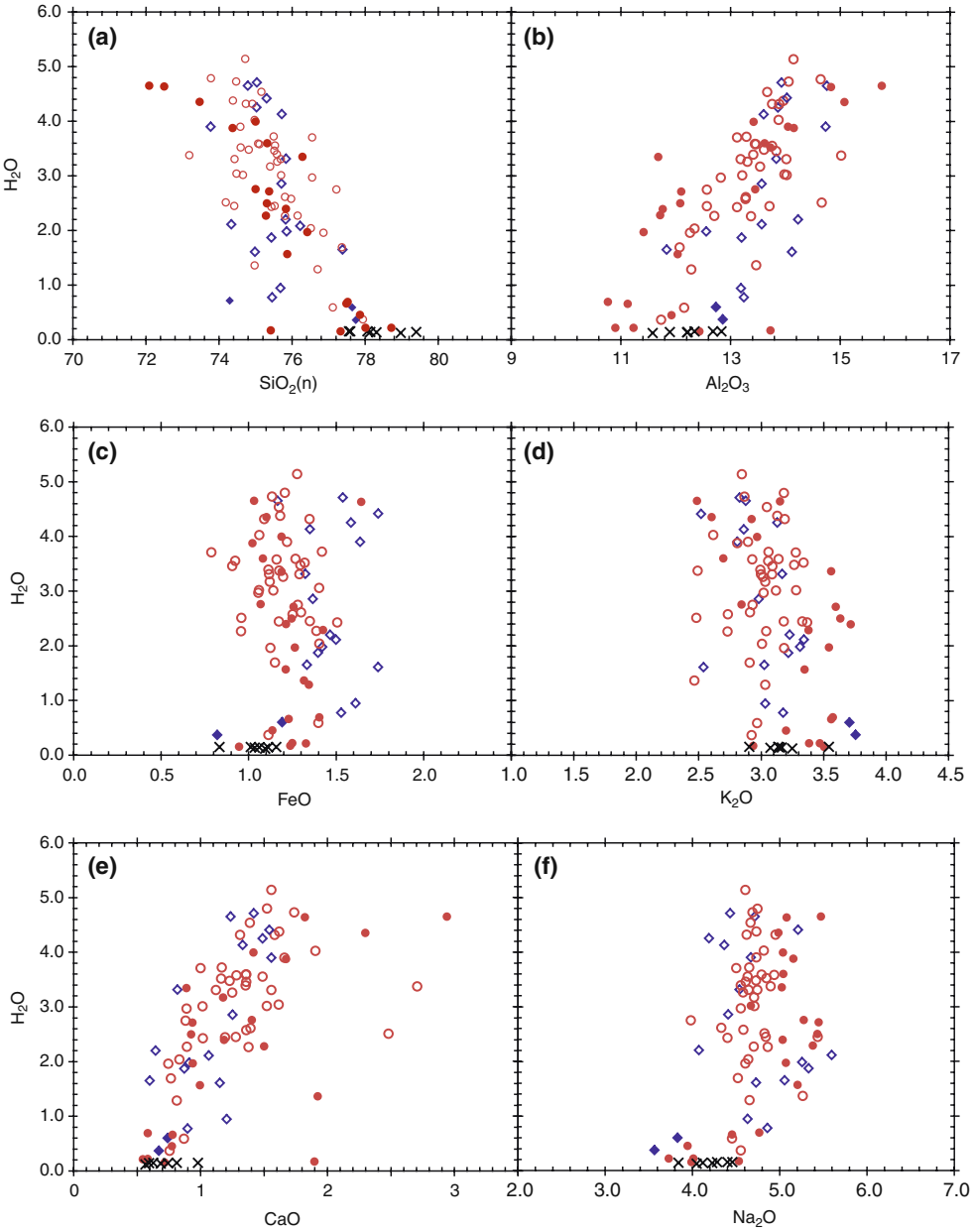

Fig. 4 Variation of melt inclusion H_2O concentrations (wt%, measured by SIMS) with anhydrous major element composition. *Open symbols* pumice, *closed symbols* dome material, *crosses-marix glasses circles* inclusions in plagioclase, *crosses-marix glasses diamonds* inclusions in hornblende

melt, to the inferred low-pressure crystallising assemblage. The major element trends in melt inclusions are consistent with a crystallising assemblage dominated by plagioclase (Fig. 3). The melt inclusions record compositions slightly more evolved than the inflection point, suggesting that a small amount (few %) of crystallisation is required before inclusions can be trapped.

Whole-rocks from the 2001 to 2004 eruption lie at silica-rich compositions compared with older eruptions and define a linear trend with SiO_2. However, rocks from previous eruptions also define linear trends, which overlap with the 2001–2004 whole-rocks. The whole-rock trends do not therefore represent a simple liquid line of descent, but rather a number of individual pulses of magmatic activity, which have undergone related processes prior to shallow-level storage and eruption (Cox et al. 1979; Eichelberger et al. 2006). In contrast, the melt inclusion population represents a true liquid line of descent, reflecting the late stages of crystallisation at low pressures in the shallow magmatic system.

The melt inclusions contain up to 5.1 wt% H_2O. Assuming H_2O-saturation, these concentrations correspond to minimum trapping pressures up to ~160 MPa (calculated at 900°C using Newman and Lowenstern 2002). We have not measured CO_2 contents of melt inclusions, however ~200 ppm dissolved CO_2 in the melt would increase the calculated pressures by ~30 MPa at the highest H_2O concentrations. This implies magma storage at ~6–7 km depth.

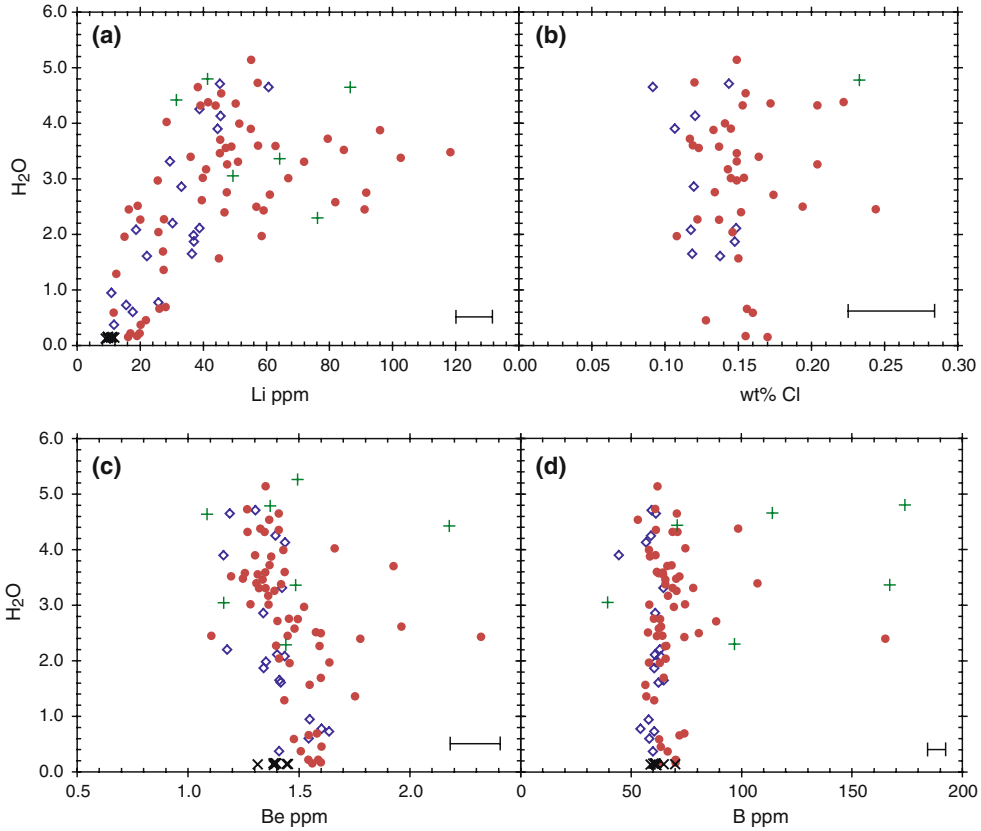

Fig. 5 Variation of light trace elements Li, Cl, Be and B with H_2O (SIMS). Cl concentrations were measured using EPMA. **a** Li correlates with H_2O. Inclusions in plagioclase are variably enriched in Li at intermediate H_2O (see text for discussion). **b** Cl and **c** Be concentrations increase slightly with decreasing H_2O. **d** B show little variation with H_2O. Some inclusions show anomalous enrichment in Be and/or B. Accuracy is estimated to be ~0.15 wt% for H_2O. Trace elements in plagioclase-hosted inclusions are not corrected for post-entrapment crystallisation. *Symbols* as for Fig. 2, except for *pluses* (exotic melts, see text)

Pure CO_2 fluid inclusions at Shiveluch were also reported by Tolstykh et al. 2000, with estimated trapping pressures of ~30–130 MPa at 900°C (Dirksen et al. 2006). Matrix glasses contain as little as 0.11 wt% H_2O, equivalent to a pressure of <1 MPa. The trapped glasses therefore record a history of low-pressure crystallisation, from a storage region at a little over 6 km depth (assuming a crustal density of 2,600 kg m^{-3}), to the surface.

Decompression crystallisation

Shiveluch magmas are not saturated in quartz or alkali feldspar, so increasing SiO_2 or K_2O in the residual melt indicates progressive crystallisation. The range of Si, K compositions recorded in the melt inclusions (see Fig. 3) therefore reflects entrapment of the inclusions at various stages of the crystallisation process. This compositional range cannot result from variable degassing of hydrous melts, because the major element concentrations presented are calculated H_2O-free (Fig. 3, Supplementary Table 1). The compositional vectors on Figs. 3 and 6 further demonstrate that the variations cannot be a result of post-entrapment crystallisation. We also reject the possibility that the chemical trends reflect mixing between a cool, Na-, Al-, Li-, H_2O-rich, K-poor, SiO_2-poor rhyodacite and a hotter, Al-, Na-, Li-, H_2O-poor, high-K, high-SiO_2 rhyolite (geothermometry from Blundy et al. 2006), because of the very high magma viscosities ($10^{4.5}$ to 10^9 Pa·s), and the absence of compositional banding, magmatic enclaves of rhyolite, and whole-rock trends reflecting such mixing.

The melt inclusions also contain a wide range of H_2O concentrations, that decrease with increasing SiO_2 and K_2O (normalised to anhydrous, Fig. 10a, b). For H_2O-saturated magma, decompression crystallisation results in falling H_2O with increasing SiO_2, because H_2O solubility in the melt decreases with pressure, while crystallisation during isobaric cooling causes increased melt SiO_2 but constant H_2O (e.g. Sisson and Layne, 1993; Blundy and Cashman 2005). Post-entrapment water loss or leakage from the inclusion would result in lower H_2O without altering the SiO_2 content. The Shiveluch melt inclusions therefore record decompression-driven crystallisation during ascent from ~6 km to the surface. As discussed earlier, the high SiO_2(n) contents (up to 80 wt%) of the melt inclusions and matrix glasses are evidence for equilibration at shallow pressures, and therefore support this result.

Concentrations of immobile, incompatible trace elements (Zr, Nb) do not correlate well with H_2O, though they appear to increase slightly as H_2O decreases (Fig. 10a, b). The data are also strongly scattered, to an extent much greater than analytical uncertainty. Possible causes of scatter include real differences in magma chemistry,

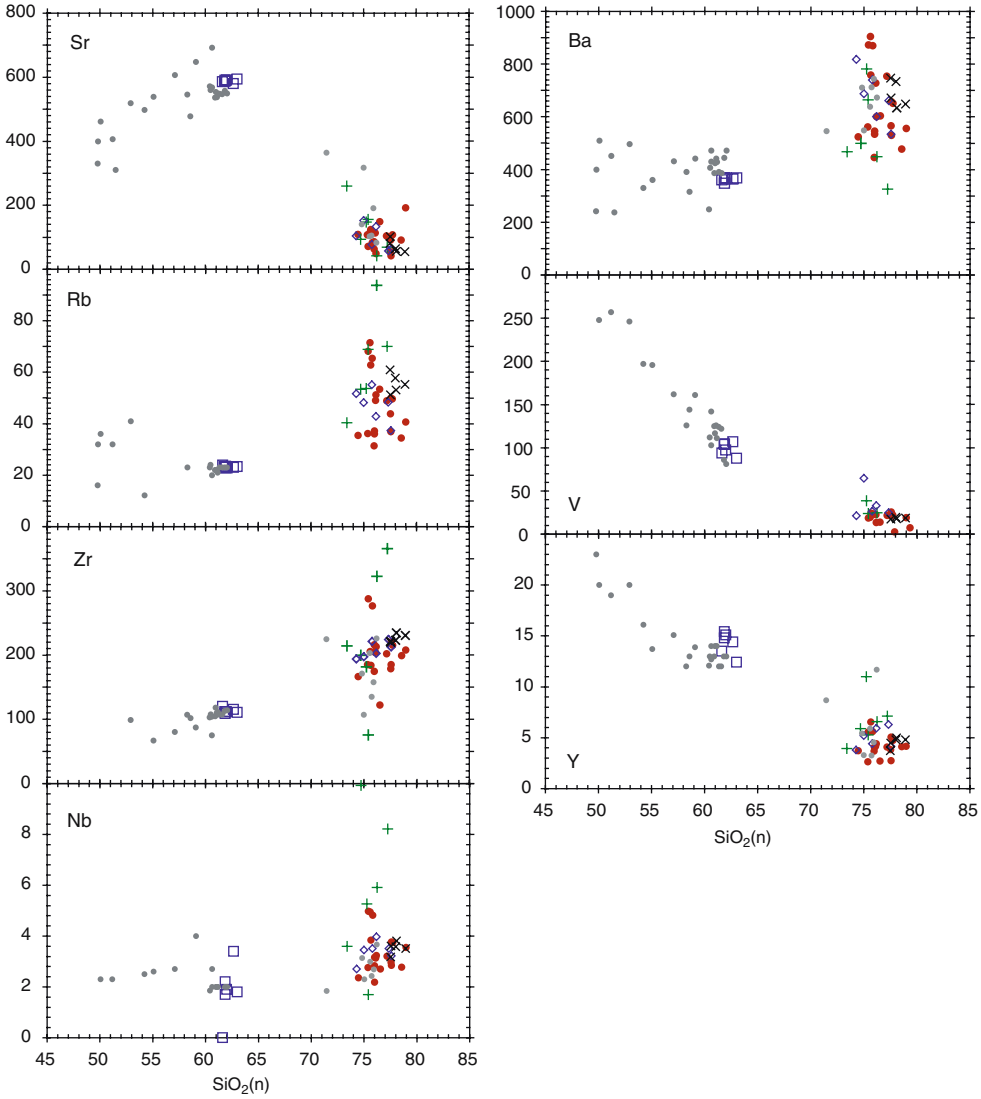

Fig. 6 Variation of trace elements (ppm) with SiO_2(wt% anhydrous) for melt inclusions and whole-rocks. *Symbols* as Fig. 5. Accuracy is estimated to be ~10% relative. Some inclusions are identified as ''exotic melts'' (*pluses*), because of their anomalous trace element behaviour (see text)

boundary layer effects (Allegre et al. 1981), spatial variations in the distribution of trace minerals (e.g. SnO_2, bornite, apatite) which could alter local bulk partition coefficients, differential amounts of post-entrapment crystallisation, sidewall crystallisation or spatial differences in crystallinity relating to temperature variations. However, given the strong variation in major elements, we would have expected to see greater variation in the concentrations of incompatible trace elements. A possible explanation is that the true variation is masked, either by initial variations in Zr and Nb between magma batches, or by a stepwise process of crystallisation, instead of a single, smooth period of ascent. Periods of ascent would be accompanied by H_2O loss, inducing crystallisation. During stagnant periods crystallisation would continue by cooling at constant pH_2O, resulting in a ''zig-zag'' H_2O-incompatible element profile. Episodic stop–start magma ascent has been documented in several eruptions (e.g. Soufrière Hills Volcano, Montserrat; Mt Unzen, Japan; Mount St Helens, USA) and can be attributed to rheological stiffening with stick–slip mechanisms (Wylie et al. 1999). Such pulsatory magma ascent is characteristic of lava dome eruptions on a variety of timescales, from hours to decades (Sparks 1997; Melnik and Sparks 2005).

The amount of decompression crystallisation occurring at Shiveluch can be estimated, assuming closed-system fractional crystallisation and using the concentration of incompatible trace elements (e.g. Zr, K, Nb) in the melt inclusions as an index of crystallinity. For simplicity, the concentration in the initial liquid was assumed to be that of the whole-rocks. The possibility that the magma crystallised zircon is excluded because, at typical pre-eruptive temperatures (840–860 °C, Humphreys et al. 2006a), zircon saturation requires 350–650 ppm Zr in the melt (Watson and Harrison 1983). Typical crystallinities vary from ~33% to ~61% and show a gradual increase as

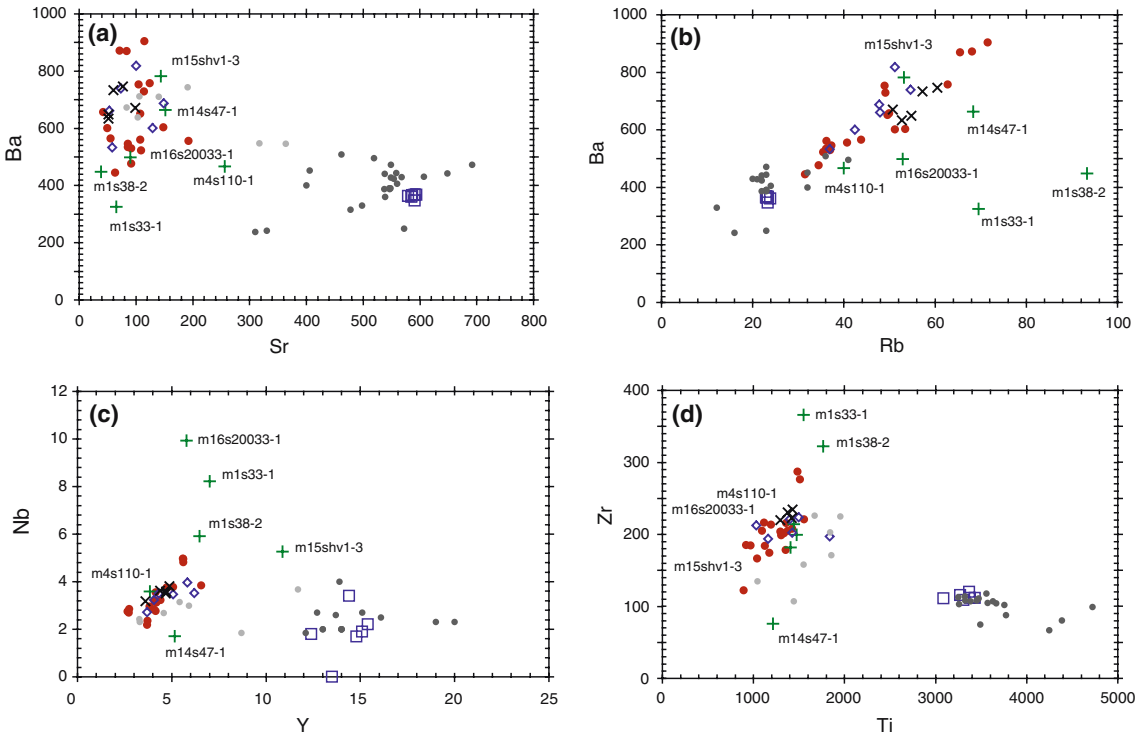

Fig. 7 Trace element plots for melt inclusions, matrix glasses and whole-rocks. *Symbols* as for Fig. 5. Pairs of trace elements with similar chemical characteristics behave consistently (e.g. LILE Rb, Ba; HFS Zr, Ti)

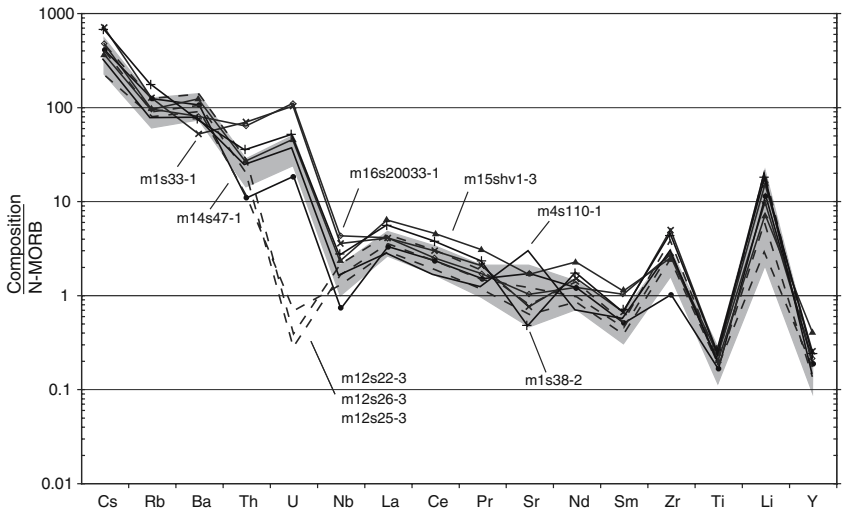

Fig. 8 MORB-normalised trace element variation diagram for melt inclusions and matrix glasses. Elements are given from *left* to *right* in order of increasing compatibility in a small fraction mantle melt (Sun and McDonough 1989). *Grey shaded field* represents the main population of melt inclusions and matrix glasses. Trace element patterns typically show high LILE and negative Nb and Ti anomalies. Variation in Sr is likely related to crystallisation of plagioclase. ''Exotic melts'' are shown and labelled individually. Melt inclusions with anomalous U/Th ratios are indicated by *dashed lines*

pressure decreases (Blundy et al. 2006). Estimated uncertainties are approximately ±4% based on the variation of whole-rock Zr. Typical crystallinities calculated using Nb range from ~23 to 53%, though whole-rock Nb values are more variable than Zr. Using K_2O to calculate *F* (fraction of melt remaining during fractional crystallisation) yields crystallinities of 53–69%. This is substantially greater than estimates using Zr and Nb; however *F* is strongly dependent on the value of whole-rock K_2O chosen. If we use the inferred initial melt value where the whole-rock and melt

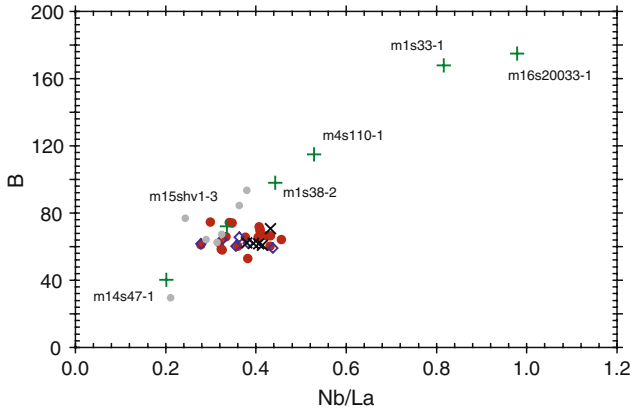

Fig. 9 B vs. Nb/La for melt inclusions and matrix glasses. Symbols as for Fig. 5. Exotic melts are easily identified by their anomalous trace element ratios, and linear co-variation of B with Nb/La

inclusion trends intersect (see earlier discussion, and Humphreys et al. 2006a), calculated crystallinities are ~30–56%, in good agreement with Zr and Nb. These calculations therefore indicate up to 25–30% decompression crystallisation.

Modal analyses and least squares calculations (Dirksen et al. 2006) indicate that a typical dome sample from Shiveluch has a total crystallinity of ~75% by volume, comprising ~45% phenocrysts and up to 30% microlites (Dirksen et al. 2006). Pumices contain ~30% phenocrysts and a few microlites. Decompression crystallisation therefore accounts for the formation of the groundmass and a small amount of phenocryst growth, implying that the magma must have already contained phenocrysts prior to ascent from 6 km depth. This is consistent with the compositional gap observed between whole-rocks and melt inclusions (see earlier). This interpretation is also supported by textural features suggesting remobilisation of crystals from cumulates or residues of earlier high-pressure crystallisation (Humphreys et al. 2006a). Remobilisation of old crystals has also been inferred in a number of previous studies (e.g. Tatara-San Pedro, Chile, Dungan et al. 2001; Crater Lake, Oregon, Bacon and Lowenstern 2005; Mount St Helens, Blundy and Cashman 2005).

Decompression crystallisation seals off melt pockets trapped in the phenocrysts. We propose that this occurs by the mechanism described in Fig. 11 (a, b). Channels of melt are commonly observed to emanate from inclusions (Fig. 11c). This suggests that inclusions were connected to the external matrix for some time before being sealed off. The inclusions therefore maintain contact with the matrix and can remain in equilibrium by exchanging chemical components (including H_2O). The stage at which the inclusion is finally sealed depends on the size of the channel, and determines the H_2O concentration recorded. Inclusions that remained connected until eruption would record the same H_2O concentration as the matrix glass. Wide channels may allow partial devitrification (Fig. 11d). The degree to an element is able to re-equilibrate with the matrix during this process should depend on its diffusivity in the melt, and the time available. We would therefore expect rapidly diffusing species (H_2O, Li, Na; Zhang 1999; Jambon 1982) to be in equilibrium with the matrix, while more slowly diffusing species (e.g. Ti, Ba, REE; Jambon 1982; Mungall et al. 1999) may tend towards a post-entrapment crystallisation signature. This may in part explain the scattered trace element trends observed. However, a detailed analysis is beyond the scope of this study.

Oxidation of hornblende-hosted inclusions

Inclusions in hornblende contain as little as 0.4 wt% H_2O. Recent experimental studies on similar magma compositions (the Mount Unzen dacite, Sato et al. 1999; Holtz et al. 2005) indicate that amphibole is stable to ~40 MPa at 800°C, or ~70 MPa at 875°C. These pressures equate to approximately 2.4 wt% H_2O at 800°C and 3.1 wt% H_2O at 875°C, assuming H_2O saturation. This suggests that crystallisation was rapid enough that breakdown rims could not form (Rutherford and Hill 1993; Browne and Gardner 2002).

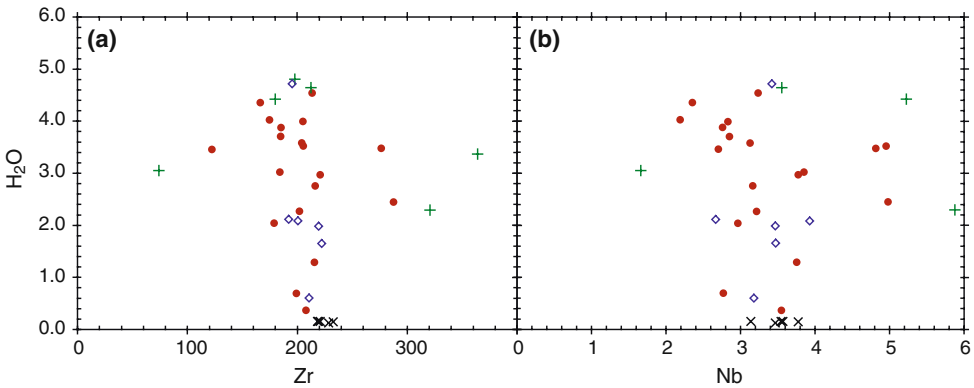

Fig. 10 H_2O vs. immobile, incompatible trace elements in melt inclusions and matrix glasses. Degree of trace element variation is less than expected. True variations may be masked by variations in Zr, Nb concentrations between magma batches, or by pulsatory ascent (see text). *Symbols* as for Fig. 5

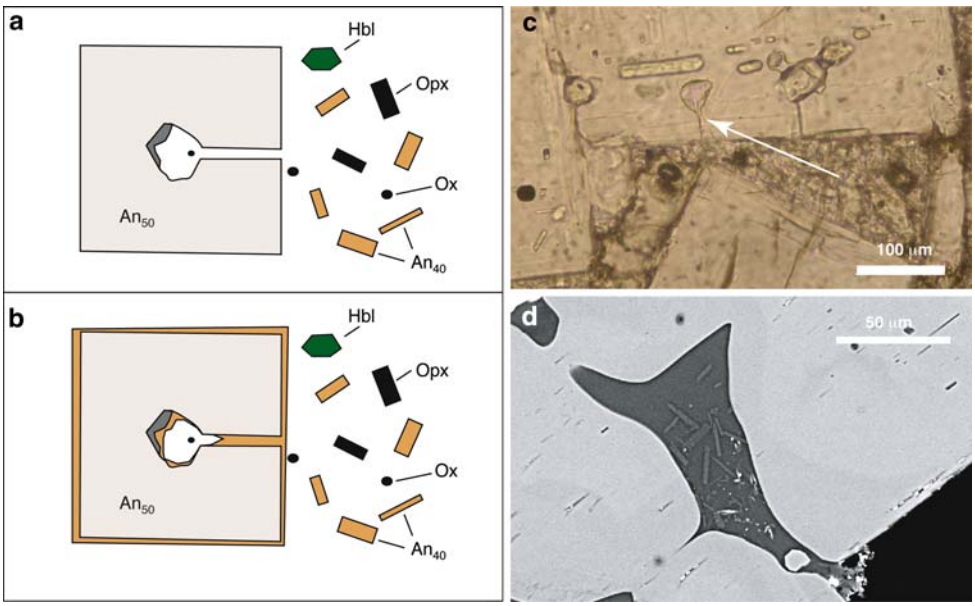

Fig. 11 Mechanism for entrapment of melt inclusions. Inclusions are connected to the external melt for some time prior to eventual sealing, and may remain in equilibrium with the matrix melt by diffusive exchange of components. While the melt channel remains open, chemical components exchange between inclusion and matrix such that the inclusion chemistry follows the same liquid line of descent as the matrix, even though the inclusion contains no mafic minerals. Some precipitation of plagioclase may occur on the walls of the inclusion during this time. Once the melt channel is finally occluded, either by precipitated plagioclase or by rim overgrowth, the inclusion finally becomes chemically isolated from the matrix melt and the two liquids no longer evolve in chemical harmony. Some inclusions never become sealed from the matrix, such as those shown in **c** (*white arrow*, in plagioclase) and **d** (in hornblende). These inclusions may preserve exactly the same composition as the matrix glass itself. Wide channels (**d**) may allow partial devitrification of the inclusion

Many hornblende-hosted inclusions also have anomalously low MgO and high FeO concentrations compared with inclusions in plagioclase (see Fig. 3). This is not consistent with post-entrapment crystallisation of hornblende, which would produce low FeO *and* MgO. These anomalous compositions could be explained by ion exchange between hornblende and included melt, caused by rapid H_2O loss during diffusive exchange with the matrix, and/or H_2O leakage along cleavage planes. Oxidation occurs during dehydration of the melt (Candela 1986; Gaillard et al. 2002; Rowe et al. 2006), resulting in decreased activity of Fe^{2+} relative to Fe^{3+}. Experiments on the Pinatubo melt showed very short timescales for melt oxidation by this mechanism (minutes to hours at 800°C, Gaillard et al. 2002). Re-equilibration between host and inclusion involves exchange of Fe^{2+} for Mg^{2+}, which could produce the anomalously high FeO and low MgO observed in hornblende-hosted melt inclusions. Plagioclase-hosted inclusions are unaffected because of poorer cleavage in plagioclase, which minimises H_2O leakage, and low concentrations of Fe and Mg in the host mineral.

''Exotic'' melts

A minority of inclusions, here termed ''exotic melts'', have anomalous trace element characteristics. One type has normal trace element concentrations but anomalously low U/Th. The other type shows highly variable HFS concentrations and correlation of B with Nb/La, or enriched REE.

Low U/Th requires removal of U without affecting other immobile, incompatible elements (e.g. Th, Zr). The most likely mechanism for producing this signature is extraction of U by a fluid under oxidising conditions (Hawkesworth et al. 1997). U^{6+} is fluid-mobile and requires strongly oxidising conditions [e.g. $\log f(O_2)$~HM (Schreiber 1983)]. This is much more oxidising than the conditions in the magma ($\leq$ NNO + 2, Humphreys et al. 2006a) and suggests a hydrothermal system. Interaction of hydrothermal fluids with isolated parts of the magmatic system could explain the limited occurrence. A similar scenario was envisaged by Harford and Sparks (2001) to explain variable D/H ratios of some amphibole phenocrysts at the Soufrière Hills Volcano, Montserrat, W. Indies. There, a proportion of the amphiboles was inferred to have cooled, solidified and interacted with hydrothermal fluids, before being remobilised and erupted in a new magma batch.

The origin of the second group of exotic melts is less clear. Hornblende-hosted inclusion m15shv1-3 is enriched in REE (which could indicate that the analysis was contaminated by hornblende), but has normal levels of Zr, V and Ti. The other inclusions behave relatively coherently on trace element plots, so any satisfactory explanation must

account for both depletion and enrichment of trace elements. This rules out extreme post-entrapment crystallisation or remobilisation of these crystals from partially solidified marginal rocks or a crystal mush (e.g. Charlier et al. 2005), since neither of these processes could produce trace element depletion. Assimilation of crustal rocks is considered unlikely because of the co-variation of Nb/La with B, which is transported by slab-derived fluids (Leeman and Sisson 1996).

A plausible explanation is that the inclusions originated from batches of magma that have differing trace element (mainly HFS) concentrations or ratios derived from a deep source. Elements such as Nb, La have similar bulk partition coefficients during mantle melting, so variations in Nb/La reflect heterogeneity in the source melt (Bougault et al. 1980), possibly through mixing or contamination. Variations in Ba/Th and B suggest varying fluid inputs. We therefore suggest that the heterogeneity could be produced by melting of heterogeneously fluid-modified mantle wedge (Rose et al. 2001). This implies that the exotic melt inclusions represent a source signature, which is preserved in the melt despite protracted late stage crystallisation and magma mixing (e.g. Humphreys et al. 2006a). The exotic compositions account for approximately 12% of the inclusions analysed for heavy trace elements. We anticipate that other anomalously high-B inclusions (not analysed for heavy trace elements) might also show an exotic trace element signature.

The whole-rocks are rather limited in composition compared with the melt inclusions, as observed in numerous other studies (e.g. Gurenko et al. 2005). This is consistent with many small batches of magma entering the subvolcanic magma system and mixing. Each magma batch differentiates at depth and ascends with slight initial variations in trace element chemistry, but experiences similar shallow-pressure conditions. The crystallising assemblage, and the whole-rock, residual melt and phenocryst compositions are therefore very similar in each sample. This is consistent with the recent model of intermediate arc magma genesis (Annen et al. 2006). The source-derived trace element characteristics of each ascending magma parcel are modified by varying degrees of fractionation, giving diverse trace element characteristics in melt inclusions. However, whole-rock magma compositions become homogenised relatively quickly, and evidence for individual increments of magma with subtle chemical characteristics is lost.

Shallow-level degassing

Li and Be concentrations record subtle features related to the shallow-level degassing. Although Li contents of hornblende-hosted inclusions correlate with H_2O, Li contents of plagioclase-hosted inclusions have a large ''tail'' to very high Li (e.g. 120 ppm, see Fig. 5a; see also Tolstykh et al. 2000) at intermediate pH_2O (2.5–4 wt% $H_2O \approx$ 40–100 MPa). This requires the magma to become enriched in Li without changes in pH_2O. A similar phenomenon is seen at Mt St Helens (Berlo et al. 2004), where it is attributed to vapour-mediated transfer of Li from a deeper reservoir to the magma. Continued degassing of magma in a deeper reservoir allows Li-rich vapour to ascend and accumulate in temporarily stalled magma in the conduit (Berlo et al. 2004). The enrichment of Li at a specific H_2O concentration suggests a pressure-mediated process, possibly condensation of a homogeneous magmatic vapour to a dense brine and low-density H_2O-rich vapour during decompression (Kent et al. 2007). If Li diffuses right through the crystal (Berlo et al. 2004; Kent et al. 2007), the lack of Li-enrichment in hornblende-hosted melt inclusions may be related to lower diffusivity compared with plagioclase. Li diffusivity in plagioclase is known to be very rapid (Giletti and Shanahan 1997). Alternatively, hornblende crystallisation may have largely ceased by the time the magma has reached intermediate pressures, preventing entrapment of Li-rich melt inclusions in hornblende.

Anhydrous Na_2O concentrations in melt inclusions decrease strongly with increasing SiO_2 (see Fig. 2g). This strong Na_2O decrease is inconsistent with crystallisation of groundmass plagioclase (Fig. 2) and suggests that a sodium-rich species is partitioned into a vapour or brine with Li. This is supported by the co-variation of Li with Na_2O (Fig. 12a). Studies of ore and hydrothermal systems indicate that chloride species are a likely constituent (e.g. Candela and Piccoli 1995; Webster 1997; Williams-Jones and Heinrich 2005), though our data are inconclusive (Fig. 12b). The fluid(s) produced by degassing of the magma contain compounds of trace metals including Na and Li. This is consistent with observations of high concentrations of mobile, volatile trace metals such as Hg in volcanic plumes (e.g. Pyle and Mather 2003), and observations of heavy metal mineralisation in sublimates of fumaroles, e.g. Re sulphides at Kudriavy volcano, Kuriles (Korzhinsky et al. 1994).

The co-variation of B with Nb/La in the exotic melts (Fig. 9) suggests that B concentrations are derived from source characteristics. In contrast, the source of enrichment in Be (see Fig. 5) at intermediate pH_2O is currently unexplained. Be partitions into the melt in preference to the vapour (Fig. 5c), and does not correlate with Li (Fig. 12c), so it is unlikely that Be could also be supplied by fluids produced at depth. However, because Be does not correlate with B, source variation also seems unlikely.

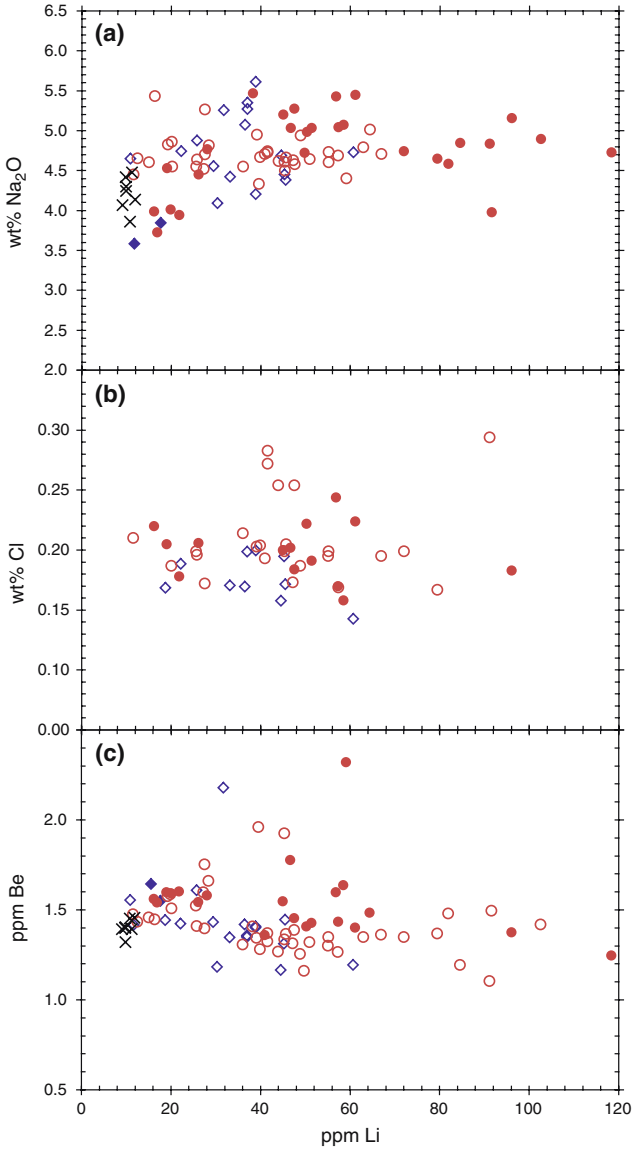

Fig. 12 Volatile element (Na, Cl, Be, Li) concentrations in melt inclusions. *Symbols* as for Fig. 4

Conclusions

Major- and trace-element concentrations and H_2O contents of melt inclusions from Shiveluch Volcano indicate decompression-induced crystallisation of a volatile-saturated magma. Modelling of immobile, incompatible trace elements indicate that decompression crystallisation accounts for formation of the groundmass and growth of phenocryst rims. Formation of phenocrysts therefore occurs primarily in the magma chamber prior to ascent. Some additional material is entrained from cumulates or deep crystallisation products, and magma mixing. Melt inclusions in hornblende are less H_2O-rich than those in plagioclase consistent with partial H_2O leakage after entrapment. This caused oxidation of hornblende-hosted inclusions, resulting in anomalous FeO, MgO concentrations.

A number of ''exotic melts'' can be identified through their normal major element compositions but anomalous incompatible trace element ratios and concentrations. The exotic melts are inferred to reflect initial variations in trace element chemistry between different magma batches, the trace element composition being derived from the deep source. Anomalous trace element ratios are preserved through magma evolution because the low pressure evolution of each magma batch is very similar. Thus the melt inclusions record processes which cannot be detected in whole-rock compositions. Scattered trace element trends could reflect punctuated decompression (ascent) and cooling (stalling). Melt pH_2O remains constant as the magma cools and crystallises, during periods of stagnation, whereas pH_2O falls during decompression crystallisation.

Li systematics indicate continuous release of vapour during degassing of magma at depth. Co-variation of Li and Na may indicate the presence of a brine at low pressure. Metals are probably transferred into the fluid as chloride complexes. The fluids may condense and re-equilibrate with temporarily stalled magma at higher levels, resulting in melts enriched in trace metals at intermediate pressures.

Acknowledgements MCSH was supported by a NERC PhD studentship and JDB by a NERC Senior Research Fellowship. RSJS acknowledges the support of a Royal Society Wolfson Merit Award. We are very grateful to Richard Hinton, Simone Kasemann and John Craven (Ion Microprobe Facility, University of Edinburgh) for assistance with ion microprobe analysis, and to Stuart Kearns (University of Bristol) for assistance with EPMA. The manuscript was improved by reviews by Maxim Portnyagin and an anonymous reviewer.

References

Allegre CJ, Provost A, Jaupart C (1981) Oscillatory zoning: a pathological case of crystal growth. Nature 294:223–228

Annen C, Blundy JD, Sparks RSJ (2006) The genesis of intermediate and silicic magmas in deep crustal hot zones. J Petrol 47:515–539

Bacon CR, Lowenstern JB (2005) Late Pleistocene granodiorite source for recycled zircon and phenocrysts in rhyodacite lava at Crater Lake, Oregon. Earth Planet Sci Lett 233:277–293

Barmin A, Melnik O, Sparks RSJ (2002) Periodic behavior in lava dome eruptions. Earth Planet Sci Lett 199:173–184

Berlo K, Blundy J, Turner S, Cashman K, Hawkesworth C, Black S (2004) Geochemical precursors to volcanic activity at Mount St Helens, USA. Science 306:1167–1169

Blundy J, Cashman K (2001) Ascent-driven crystallisation of dacite magmas at Mount St Helens, 1980–1986. Contrib Mineral Petrol 140:631–650

Blundy J, Cashman K (2005) Rapid decompression-driven crystallization recorded by melt inclusions from Mount St Helens volcano. Geology 33:793–796

Blundy J, Cashman K, Humphreys M (2006) Magma heating by decompression-driven crystallization beneath andesite volcanoes. Nature 443:76–80

Bougault H, Joron JL, Treuil M (1980) The primordial chondritic nature and large-scale heterogeneities in the mantle: evidence from high and low partition coefficient elements in oceanic basalts. Phil Trans R Soc Lon A 297:203–213

Browne BL, Gardner JE (2002) Experimental calibration of amphibole breakdown rates in response to decompression and heating. EOS Trans AGU 83:F1464

Candela PA (1986) The evolution of aqueous vapour from silicate melts: effect on oxygen fugacity. Geochim Cosmochim Acta 50:1205–1211

Candela P, Piccoli P (1995) Model ore-metal partitioning from melts into vapor and vapor/brine mixtures. In: Thompson JFH (ed) Granites, fluids and ore deposits. Mineral Assoc Canada 23:101–128

Cashman KV (1992) Groundmass crystallization of Mount St Helens dacite, 1980–1986: a tool for interpreting shallow magmatic processes. Contrib Mineral Petrol 109:431–449

Cashman K, Blundy J (2000) Degassing and crystallization of ascending andesite and dacite. Phil Trans R Soc Lond A 358:1487–1513

Charlier BLA, Wilson CJN, Lowenstern JB, Blake S, van Calsteren PW, Davidson JP (2005) Magma generation at a large, hyperactive silicic volcano (Taupo, New Zealand) revealed by U-Th and U-Pb systematics in zircons. J Petrol 46:3–32

Clocchiatti R (1975) Les inclusions vitreuses des cristaux de quartz. Etude optique, termo-optique et chimique. Applications geologiques. Mem Soc Geol France 54

Cottrell E, Spiegelman M, Langmuir CH (2002) Consequences of diffusive reequilibration for the interpretation of melt inclusions. Geochem Geophys Geosys 3:doi:10.1029/2001GC000205

Cox KG, Bell JD, Pankhurst RJ (1979) The interpretation of igneous rocks. George Allen & Unwin Ltd., London, p 450

Devine JD, Gardner JE, Brack HP, Layne GD, Rutherford MJ (1995) Comparison of microanalytical methods for estimating H_2O contents of silicic volcanic glasses. Am Mineral 80:319–328

Dirksen O, Humphreys MCS, Pletchov P, Melnik O, Demyanchuk Y, Sparks RSJ, Mahony S (2006) The 2001–2004 dome-forming eruption of Shiveluch volcano, Kamchatka: Observation, petrological investigation and numerical modelling. J Volcanol Geotherm Res 155:201–226

Dungan MA, Wulff A, Thompson R (2001) Eruptive stratigraphy of the Tatara-San Pedro Complex, 36°S, Southern Volcanic Zone, Chilean Andes: Reconstruction method and implications for magma evolution at long-lived arc volcanic centers. J Petrol 42:555–625

Eichelberger JC, Izbekov PE, Browne BL (2006) Bulk chemical trends at arc volcanoes are not liquid lines of descent. Lithos 87:135–154

Frezzotti M-L (2001) Silicate melt inclusions in magmatic rocks: applications to petrology. Lithos 55:273–299

Gaetani GA, Watson EB (2000) Open system behavior of olivine-hosted melt inclusions. Earth Planet Sci Lett 183:27–41

Gaillard F, Scaillet B, Pichavant M (2002) Kinetics of iron oxidation-reduction in hydrous silicic melts. Am Min 87:829–837

Geschwind C-H, Rutherford MJ (1995) Crystallization of microlites during magma ascent: the fluid mechanics of 1980–1986 eruptions at Mount St Helens. Bull Volcanol 57:356–370

Gill JB (1981) Orogenic andesites and plate tectonics. Springer, Berlin, p 358

Giletti BJ, Shanahan T (1997) Alkali diffusion in plagioclase felspar. Chem Geol 139:3–20

Gioncada A, Clocchiatti R, Sbrana A, Bottazzi P, Massare D, Ottolini L (1998) A study of melt inclusions at Vulcano (Aeolian Islands, Italy): insights on the primitive magmas and on the volcanic feeding system. Bull Volcanol 60:286–306

Gurenko AA, Trumbull RB, Thomas R, Lindsay JM (2005) A melt inclusion record of volatiles, trace elements and Li-B isotope variations in a single magma system from the Plat Pays Volcanic Complex, Dominica, Lesser Antilles. J Petrol 46:2495–2526

Harford CL, Sparks RSJ (2001) Recent remobilisation of shallow-level intrusions on Montserrat revealed by hydrogen isotope composition of amphiboles. Earth Planet Sci Lett 185:285–297

Hawkesworth C, Turner S, Peate D, McDermott F, van Calsteren P (1997) Elemental U and Th variations in island arc rocks: implications for U-series isotopes. Chem Geol 139:207–221

Hochstaedter AG, Kepezhinskas P, Defant M, Drummond M (1996) Insights into the volcanic arc mantle wedge from magnesian lavas from the Kamchatka arc. J Geophys Res 101(B1):697–712

Holtz F, Johannes W (1994) Maximum and minimum water contents of granitic melts: implications for chemical and physical properties of ascending magmas. Lithos 32:149–159

Holtz F, Sato H, Lewis J, Behrens H, Nakada S (2005) Experimental petrology of the 1991–1995 Unzen dacite, Japan. Part I: phase relations, phase composition and pre-eruptive conditions. J Petrol 46:319–337

Humphreys MCS, Blundy JD, Sparks RSJ (2006a) Magma evolution and open-system processes at Shiveluch Volcano: Insights from phenocryst zoning. J Petrol 47:2303–2334

Humphreys MCS, Kearns S, Blundy JD (2006b) SIMS investigation of electron-beam damage to hydrous, rhyolitic glasses: implications for melt inclusion analysis. Am Mineral 91:667–679

Ishikawa T, Tera F, Nakazawa T (2001) Boron isotope and trace element systematics of the three volcanic zones in the Kamchatka arc. Geochim Cosmochim Acta 65:4523–4537

Jambon A (1982) Tracer diffusion in granitic melts: experimental results for Na, K, Rb, Cs, Ca, Sr, Ba, Ce, Eu to 1300°C and a model of calculation. J Geophys Res 87:10797–10810

Kent AJR, Blundy J, Cashman K, Cooper KM, Donnelly C, Pallister JS, Reagan M, Rowe MC, Thornber CR (2007) Vapor transfer prior to the October 2004 eruption of Mount St Helens, Washington. Geology 35:231–234

Kepezhinskas P, McDermott F, Defant MJ, Hochstaedter A, Drummond MS, Hawkesworth CJ, Koloskov A, Maury RC, Bellon H (1997) Geochim Cosmochim Acta 61:577–600

Korzhinsky MA, Tkachenko SI, Shmulovich KI, Taran YA, Steinberg GS (1994) Discovery of a pure rhenium mineral at Kudriavy volcano. Nature 369:51–52

Leeman WP, Sisson VB (1996) Geochemistry of boron and its implications for crustal and mantle processes. Rev Mineral Geochem 33:645–707

Lowenstern JB (2003) Melt inclusions come of age: volatiles, volcanoes and Sorby's legacy. In: De Vivo B, Bodnar RJ (eds) Melt inclusions in volcanic systems: methods, applications and problems. Dev Volcanol 5:1–22

Martin V (2001) Petrology of andesite from Shiveluch Volcano, Kamchatka and a comparison with Soufrière Hills Volcano, Montserrat. Unpublished MSc thesis, University of Bristol, Bristol, 68pp

Melekestsev IV, Volynets ON, Yermakov VA, Kirsanova TP, Masurenkov YP (1991) Sheveluch volcano. In: Fedotov SA, Masurenkov YP (eds) Active volcanoes of Kamchatka. Nauka, Moscow pp 84–105

Melnik O, Sparks RSJ (2005) Controls on conduit magma flow dynamics during lava dome building eruptions. J Geophys Res 110:B02209

Metrich N, Rutherford MJ (1992) Experimental study of chlorine behaviour in hydrous silicic melts. Geochim Cosmochim Acta 56:607–616

Mungall JE, Dingwell DB, Chaussidon M (1999) Chemical diffusivities of 18 trace elements in granitoid melts. Geochim Cosmochim Acta 63:2599–2610

Nakamura M, Shimakita S (1998) Dissolution origin and syn-entrapment compositional change of melt inclusion in plagioclase. Earth Planet Sci Lett 161:119–133

Naumov BV, Kovalenko VI, Babanskii AD, Tolstykh ML (1997) Genesis of andesites: evidence from studies of melt inclusions in minerals. Petrology 5:586–596

Newman S, Lowenstern JB (2002) VolatileCalc: a silicate melt-H_2O-CO_2 solution model written in Visual Basic for Excel. Comp Geosci 28:597–604

Pineau F, Semet MP, Grassineau N, Okrugin VM, Javoy M (1999) The genesis of the stable isotope (O,H) record in arc magmas: the Kamtchatka's case. Chem Geol 135:93–124

Pyle DM, Mather TA (2003) The importance of volcanic emissions for the global atmospheric mercury cycle. Atmos Environ 37:5115–5124

Qin Z, Lu F, Anderson AT (1992) Diffusive reequilibration of melt and fluid inclusions. Am Mineral 77:565–576

Roedder E (1984) Fluid inclusions. Rev Mineral 12:644

Rose EF, Shimizu N, Layne GD, Grove TL (2001) Melt production beneath Mt Shasta from Boron data in primitive melt inclusions. Science 293:281–283

Rowe MC, Nielsen RL, Kent AJR (2006) Anomalously high Fe contents in rehomogenized olivine-hosted melt inclusions from oxidized magmas. Am Mineral 91:82–91

Rutherford MJ, Hill PM (1993) Magma ascent rates from amphibole breakdown: an experimental study applied to the 1980–1986 Mount St Helens eruptions. J Geophys Res 98:19667–19685

Sato H, Nakada S, Fujii T, Nakamura M, Suzuki-Kamata K (1999) Groundmass pargasite in the 1991–1995 dacite of Unzen volcano: phase stability experiments and volcanological implications. J Volc Geotherm Res 89:197–212

Schreiber HD (1983) The chemistry of uranium in glass-forming aluminosilicate melts. J Less Common Metals 91:129–147

Sisson TW, Layne GD (1993) H_2O in basalt and basaltic andesite glass inclusions from four subduction-related volcanoes. Earth Planet Sci Lett 117:619–635

Sparks RSJ (1997) Causes and consequences of pressurisation in lava dome eruptions. Earth Planet Sci Lett 150:177–189

Sparks RSJ, Pinkerton H (1978) Effect of degassing on rheology of basaltic lava. Nature 276:385–386

Sparks RSJ, Murphy MD, Lejeune AM, Watts RB, Barclay J, Young SR (2000) Control on the emplacement of the andesite lava dome of the Soufrière Hills Volcano, Montserrat by degassing-induced crystallisation. Terra Nova 12:14–20

Sun SS, McDonough WF (1989) Chemical and isotopic systematics of oceanic basalts: implications for mantle compositions and processes. In: Saunders AD, Norry MJ (eds) Magmatism in ocean basins. Geol Soc Lon Spec Publ 42:313–345

Swanson SE, Naney MT, Westrich HR, Eichelberger JC, (1989) Crystallization history of Obsidian Dome, Inyo Domes, California. Bull Volcanol 51:161–176

Tolstykh ML, Naumov VB, Babansky AD, Khubanaya SA, Kononkova NN (2000) Chemical composition, trace elements, and volatile components of melt inclusions in minerals from andesites of the Shiveluch volcano, Kamchatka. Geochem Inter 38:S123–S132

Tsuchiyama A (1985) Dissolution kinetics of plagioclase in the melt of the system diopside-albite-anorthite, and origin of dusty plagioclase in andesites. Contrib Mineral Petrol 89:1–16

Tuttle OF, Bowen NL (1958) Origin of granite in the light of experimental studies in the system $NaAlSi_3O_8$–$KAlSi_3O_8$—-SiO_2—H_2O. Geol Soc Am Mem 74:153

Volynets ON, Ponomareva VV, Babansky AD (1997) Magnesian basalts of Shiveluch andesite volcano, Kamchatka. Petrology 5:183–196

Watson EB (1976) Glass inclusions as samples of early magmatic liquid: determinative method and application to a South Atlantic basalt. J Volcanol Geotherm Res 1:73–84

Watson EB, Harrison TM (1983) Zircon saturation revisited—temperature and composition effects in a variety of crustal magma types. Earth Planet Sci Lett 64:295–304

Webster JD (1997) Chloride solubility in felsic melts and the role of chloride in magmatic degassing. J Petrol 38:1793–1807

Williams-Jones AE, Heinrich CA (2005) Vapor transport of metals and the formation of magmatic-hydrothermal ore deposits. Bull Soc Econ Geol 100:1287–1312

Wylie JJ, Voight B, Whitehead JA (1999) Instability of magma flow from volatile-dependent viscosity. Science 285:1883–1885

Zhang YX (1999) H_2O in rhyolitic glasses and melts: Measurements, speciation, solubility and diffusion. Rev Geophys 37:493–516